Inertial Deposition Effects: A Study of Aerosol Mechanics in the Trachea Using Laser Doppler Velocimetry and Fluorescent Dye

T. E. Corcoran
Pulmonary, Allergy, and Critical Care Medicine,
University of Pittsburgh, Pittsburgh, PA
e-mail: corcorante@msx.upmc.edu

Norman Chigier
Mechanical Engineering Dept.,
Carnegie Mellon University, Pittsburgh, PA
e-mail: chigier@andrew.cmu.edu

This study characterizes the axial velocity and axial turbulence intensity patterns noted in the tracheal portion of a cadaver-based throat model at two different steady flow rates (18.1 and 41.1 LPM.) This characterization was performed using Phase Doppler Interferometry (Laser Doppler Velocimetry). Deposition, as assessed qualitatively using fluorescent dye, is related to the position of the laryngeal jet within the trachea. The position of the jet is dependent on the downstream conditions of the model. It is proposed therefore that lung/airway conditions may have important effects on aerosol deposition within the throat. There is no correspondence noted between regions of high axial turbulence intensity and deposition. [DOI: 10.1115/1.1516572]

Introduction

The advantages of pulmonary drug delivery through the inhalation of a medicinal aerosol have recently led to the development of a series of new aerosol medications. For some medications this route is utilized because it offers topical treatment of specific lung conditions while limiting the whole-body effects. Examples of medications being given for topical treatment of the lungs include antivirals for influenza [1], cyclosporine for immunosuppression after lung transplantation [2], antibiotics for pneumonia [3] and heparin/acetylcystine mixtures for inhalation burns [4]. In some cases inhaled delivery is utilized to allow for quick and dependable access to the bloodstream through the vasculature of the lungs. Examples of inhaled medications being administered for this reason include insulin for diabetes [5,6] and opiates for pain control [7]. Many of these new medications do not have an obvious physical effect that indicates to the clinician that the drug has been delivered in sufficient dose to the proper portions of the lungs. This has prompted an increased need to understand the pulmonary deposition of aerosols in order to ensure effectiveness and proper dosing. Elements of variability include device performance and patient factors such as age, disease state, and general intersubject variability based on different breathing parameters, anatomical differences etc.

One patient related element that must be considered is deposition of the medication in the mouth and throat. Medication deposited in these regions is less available to the bloodstream and is not available for treatment of the lungs. The quantity of drug deposited in these regions has been shown to be highly variable. While administering 3.6 μm radio-tagged particles, to adult asthma patients, Svartengren et al. [8] reported total levels of mouth and throat deposition of between 9 and 76% with a mean level of 12%. (Percentages are in terms of total inhaled mass). Particularly high levels of mouth and throat deposition have been noted in pediatric patients receiving aerosol treatments. In Chua et al. [9], six children (ages 6 through 15) were administered a radioactively tagged spray. These children demonstrated average pulmonary deposition levels of 6% of the total medication. Mouth and throat deposition levels averaged 34%. Levels ranged between 15.6% and 49.4%. High levels of pharyngeal deposition were also noted in this population [10].

Contributed by the Bioengineering Division for publication in the JOURNAL OF BIOMECHANICAL ENGINEERING. Manuscript received November 2000; revised manuscript received June 2002. Associate Editor: J. B. Grotberg.

In Heyder et al. [11] "laryngeal" deposition was measured in adults using a series of monosized, radioactive aerosols. Laryngeal deposition (which likely included at least some element of pharyngeal and tracheal deposition) was not detected for particles smaller than 3 μm. Deposition levels quickly increased with particle size: 15% for 5 μm, 38% for 7 μm, 58% for 9 μm, 84% for 15 μm. Here again percentage is based on total inhaled mass.

Studies of both flow and deposition have been performed using in vitro models or casts of the mouth, throat, and central airways. Early studies of turbulence levels in the trachea were reported by West and Hugh-Jones [12] and Dekker [13]. The latter work described the onset of turbulence in a model throat. A model including the larynx demonstrated the onset of turbulence at much lower flow rates compared to a model without the larynx (6 liters/min vs. 21 liters/min). Olson et al. [14] described the study of a series of models that included the larynx, trachea and upper airways through the lobar bronchi. Hot wire anemometry was utilized to measure velocity contours in various portions of this model. A strong jet emanating from the vocal folds was apparent in the posterior trachea. The jet appeared to rotate towards the right, resulting a strong core flow into the right bronchus.

Schlesinger and Lippmann [15] considered deposition in a cast of the trachea, main, lobar, and segmental bronchi using ferric oxide particles tagged with Technetium 99 (99Tc). Good correspondence was noted between total deposition and an impaction parameter (as plotted on a log scale):

$$impaction = \rho d^2 Q \tag{1}$$

where ρ is the particle density, d is particle diameter, and Q is the inhalation flow rate. A similar relationship was noted between the deposition level in each specific generation of the bronchi and the impaction parameter, again plotted on a log scale. The authors also noted that most of the deposition occurred at the airway bifurcations. The highest levels of deposition occurred near the carina (the first bifurcation between the trachea and the main bronchi). The casts did not include larynges, which the authors consider to be a shortcoming of the work.

In a subsequent study, Schlesinger and Lippmann [16] studied deposition in the human trachea utilizing a cast model that included a model larynx. The deposition levels and deposition locations of the smallest particles tested within the human-based cast models (0.3 and 1.2 μm), varied greatly with flow rate. At the highest flow rate both classes demonstrated high deposition peaks in the trachea within 2 cm of the larynx. The authors speculated

that this deposition was caused by increased levels of turbulence within this region. The larger particles tested (up to 8 μm) demonstrated more consistent peaks in deposition generally within the first 3-4 cm of the trachea. The authors attributed these peaks mostly to the effects of direct impaction of the laryngeal jet, though turbulence is also considered a factor for all of the size classes. The deposition patterns within the casts including a model larynx were significantly different from the patterns noted in tracheal models not containing a larynx. The presence of the larynx appears to have increased the total levels of deposition, and moved the peak deposition location towards the upper portion of the trachea. Similar results for tracheal deposition were noted in Schlesinger et al. [17], which represents an expansion of the previous works to include a more detailed casting of the lung morphometry.

Several authors have considered the use of a single parameter to describe deposition within the larynx, the trachea and the upper tracheobronchial tree. The parameter chosen is the Stokes number, which is defined as:

$$Stokes = \frac{\rho d^2 V}{18 \mu D} \tag{2}$$

where ρ is droplet or particle density, d is droplet or particle diameter, V is (inhalation) velocity, μ is the viscosity of air, and D is a representative geometric parameter such as tracheal diameter. The Stokes Number represents the ratio of droplet time scale ($\rho d^2/18\mu$) to the flow time scale (D/V). Practically, it provides a gage of droplet inertia compared to the steering drag forces of the flow. A high Stokes number indicates that the droplet is more inertial and more likely to lag the effects of a flow acceleration/deceleration, change of direction, etc. These more inertial droplets are more likely to follow tangential or ballistic paths, increasing their chances of colliding with the airway surfaces.

In Martonen [18,19], the author considered his own experimental work with airway casts as well as the experimental work of other groups and proposed several relationships between deposition probability and Stokes number. For losses in the larynx he proposed:

$$\text{Deposition Probability (larynx)} = a + b\ (\text{Stokes}) \tag{3}$$

where $a = 0.0350$ and $b = 3.900$ (for $0.001 < \text{Stokes} < 0.1$). Chan et al. [20] reported a similar result, where $a = 0.0277$ and $b = 4.702$ (for $\text{Stokes} < 0.02$). The authors respectively reported correlations of $r = 0.96$ and $r = 0.91$.

In deposition tests performed in casts, Martonen noted a high level of particle capture within the trachea which he attributed to: (1) direct impaction of the particles onto the walls of the trachea by a jet created within the larynx and (2) the presence of flow instabilities caused by the laryngeal jet that subsequently cause increased deposition downstream due to turbulence related mechanisms [19]. Maximum deposition was typically noted either in the trachea or in the 3rd generation of the bronchi. Martonen and Lowe [21] further details this research.

Tracheal deposition was characterized using an empirical correlation, again in terms of Stokes number by Chan et al. [20]:

$$\text{Deposition Probability (Trachea)} = 2.536\ (\text{Stokes})^{1.231} \tag{4}$$

for $\text{Stokes} < 0.01$ with a correlation of $r = 0.88$. Martonen [19] and Chan et al. [20] both relied on a relatively small number of test cases in order to draw their correlations. In the first work, six different Stokes numbers were utilized. Variation of the Stokes number was effected by changing aerosol size (6 sizes) and flow rate (3 flow rates). Three different laryngeal casts with three different flow areas were used to change flow rate. The tracheobronchial tree was based on published morphometry results. The results of the latter work were based on 6-12 Stokes number cases, based on three different flow rates. The different flow rates were again obtained by the use of three different laryngeal casts. The tracheobronchial tree of Chan et al. [20] was based on an exact casting and included more generations than that used in Martonen [19]. The geometry of the experiment was not varied beyond changing the larynx mold during testing.

Stokes number was again utilized by Kim and Fischer [22] to describe the deposition of particles as they passed through sequential bifurcation models (simulating the carina and central airways). Deposition efficiency increased with increasing Stokes number (apx. 1% at $\text{Stokes} = 0.02$ up to 40% at $\text{Stokes} = 0.2$). This parameter was the dominant determinant of deposition regardless of changes in branching angle or branching pattern (symmetry or asymmetry). Deposition tended to be higher in the first of two sequential bifurcations, though deposition levels at both bifurcations corresponded well to Stokes number in the following form:

$$\text{Deposition Probability (Bifurcation)} = 1 - 1/(a\ \text{Stokes}^b + 1) \tag{5}$$

where a and b are constants. Different values of a and b were presented for the first and second bifurcations of the different models used. Myojo and Takaya [23] noted a Stokes relationship describing the deposition of fibers in the upper bronchi.

Cheng et al. [24] utilized an airway cast that included the upper respiratory tract from the oral cavity through the 4th generation of bronchi to study deposition levels in the oral cavity. Deposition was found to correlate with Stokes number as follows:

$$\text{Deposition Probability (Oral)} = 1 - e^{(-6.66\ \text{Stokes})} \tag{6}$$

with a correlation of $r = 0.976$. The authors suggested that that the minimum dimension near the larynx and the averaged diameter of the oral cavity were important parameters. In this case, the velocity component of the Stokes number was based on the mean cross sectional area of the oral cavity, pharynx and larynx, and a known flow rate. The geometric parameter (D in Eq. (2)) was based on the mean hydraulic diameter of the same portion of the cast.

An experimental model describing flows in the trachea was presented by Wroblewski and Choi [25]. This work considered a simple throat model with oscillating flow and examined velocity and turbulence characteristics downstream of the larynx using hot wire anemometry. The authors asserted that the turbulence created by the laryngeal jet is likely a convective effect of the flow and not an oscillatory effect of the breathing pattern. They noted that higher levels of turbulence are generated by a triangular larynx vs. a round one.

Mathematical models have been created that either quantitatively describe deposition in the throat based on a series of empirical equations, or describe deposition qualitatively based on a mathematical modeling of the flows in the region. Martonen [26] presented a comprehensive model describing aerosol deposition in terms of mechanism (impaction, sedimentation and diffusion) and location within the airways and lungs. The flow condition (laminar or turbulent flow) was also considered. A mathematical model of flow in the larynx and trachea was presented by Martonen et al. [27]. This reference also made extensive comparisons with past experimental works in order to verify the validity of the model. It proposed that deposition at the carinal ridge and high vorticity in the tracheobronchial airways might be consequences of the laryngeal jet.

Computation fluid dynamics (CFD) models have been utilized to consider fluid mechanics and aerosol deposition in the throat. The creation of a computational flow model of the throat was described by Katz and Martonen [28,29]. In this model the throat was depicted through a series of cylinders and elliptical portions representing the vocal fold region. The FIDAP computational package was used to compute the model. The first work described the salient characteristics of the flow fields around the larynx as: (1) a central jet created by the vocal folds, (2) a recirculation zone downstream of the vocal folds, (3) a circumferential secondary flow. The latter work described particle motion in the throat and how the recirculation zones can trap aerosol particles. These recirculation regions disappeared, however, when the increase in

glottal lumen that occurs at high inhalation flow rates was incorporated. The effect of the modulation of the glottis was further considered [30].

Katz et al. [31] used the model described above and the FIDAP code to study particle deposition in the larynx and trachea. Deposition was quantified in a series of bins based on longitudinal position in the larynx and trachea. When the motion of eleven 10 μm particles was modeled, heavy deposition was noted in the region above and including the glottal plane. The authors attributed this to a turbulence mechanism. Similar patterns of deposition were noted for 10 μm and 0.1 μm particles with the heaviest deposition for both particle sizes occurring upstream of the vocal folds.

Renotte et al. [32] modeled air flows through the larynx using Fluent UNS 4. The model included elliptical and triangular sections representing the laryngeal anatomy. The lumen of the model varied during the inspiration to match human conditions. At peak inspiration a clear posterior jet was noted. The jet velocity was approximately four times the inlet velocity and the jet extended for approximately 40 mm (2 diameters) into the trachea. Reverse flow regions were noted in the anterior trachea.

A computational model of a simple throat using the CFD package KIVA-3V was discussed in Gemci [33]. Here the throat was modeled as a simple tube containing a triangular constriction. The computational model was utilized to study velocity and turbulence parameters such as turbulence intensity and turbulent kinetic energy at different lengthwise locations. The motion of a large number of spray droplets (apx. 2×10^8) was considered, and spray dynamic effects such as coalescence and evaporation were incorporated. A strong jet was seen in the posterior tracheal portion of the model. Regions of recirculation were noted underneath the vocal folds, that led to higher deposition in the anterior trachea for the lower of two flow rate cases. Deposition, however, was generally heaviest on the posterior trachea. Computational results based on the model described herein are also currently being compiled. These results have been presented in a preliminary form in Gemci [34,35].

Martonen et al. [36] considered the specific effects of carinal ridge shape through the use of the FIDAP modeling package. The downstream effects of the carinal ridge varied with flow rate with only local effects occurring at lower flow rates and more sustained effects occurring at higher flow rates. Martonen et al. [37] considered the effects caused by the cartilaginous rings of the trachea, again using FIDAP. At lower flow rates (14 liters/min) the effects of the rings mostly occurred near the tracheal wall. At high flow rates (120 liters/min) the disturbances caused by the rings propagated towards the center of the trachea, causing a very narrow core flow. In general these effects are all very dependent on inhalation flow rate. A review of the state of the art of computational lung modeling can be found in Martonen et al. [38].

The present study characterizes the axial velocity patterns noted in the tracheal portion of a cadaver based model of the throat. This characterization was performed using Phase Doppler Interferometry, an optical technique that does not interfere with the flow. This axial velocity data was compiled into contours at various downstream planes within the trachea. Contours of axial turbulence intensity were also generated. The axial velocity and turbulence contours are compared to deposition data obtained using the same throat model and a nebulized, fluorescent dye. Specific tracheal deposition mechanisms are proposed.

Experimental Apparatus

A steady flow model of the lower pharynx, larynx, trachea and carina was used. A diagram of the apparatus appears in Fig. 1. The partial-pharyngeal, laryngeal, and carinal portions of the model were cast from an 84 year-old female cadaver. The casting technique was detailed within Corcoran, Chigier [39]. A glass tube was installed in place of the trachea to allow for experimental observation and measurement. The tube was thin walled glass (1

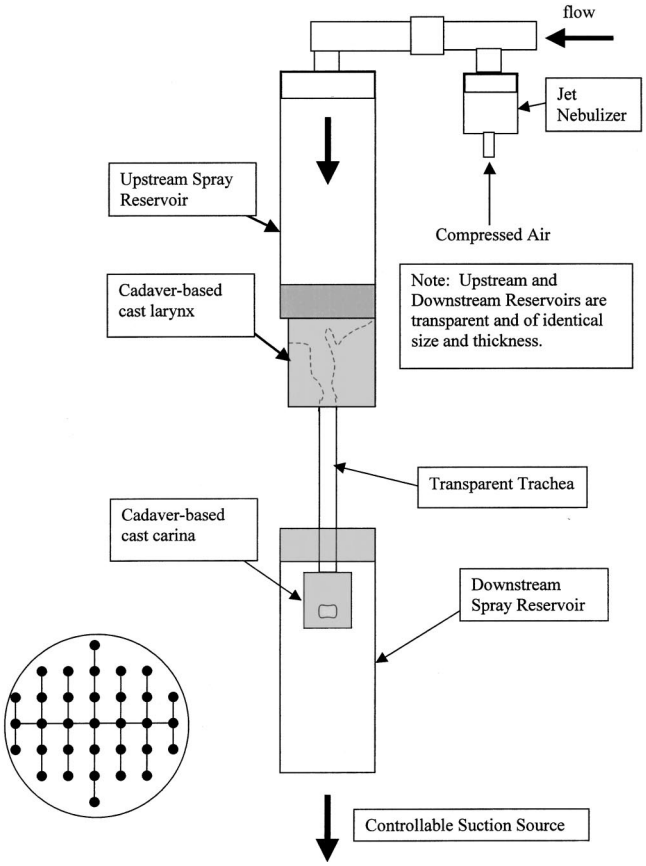

Fig. 1 Steady flow experimental apparatus incorporating laryngeal and carinal castings from a female cadaver. Axial velocity contours, axial turbulence intensity contours and qualitative deposition measurements are made in the tracheal portion of the model.

mm) and of equal diameter and length to the original trachea sample (1.5 cm in diameter and 12 cm long). The area of the model vocal fold lumen was approximately 38% the area of the trachea according to measurements ($0.60\ cm^2/1.58\ cm^2$). Wroblewski and Choi [25] reported a typical in vivo value of 40% for this area ratio at mid-inspiration. The glottal aperture will change in size during inspiration [30]. It should be understood that changes in the glottal opening associated with different phases of the inspiratory process would create a variety of different tracheal flow conditions within one breath, and that this model will simulate conditions during one instance of a complete inspiration. The length of the glottal opening was 14.2 mm compared to the average length of 22.1 mm for males and 17.5 mm for females. The area of the glottal lumen was $0.60\ cm^2$ compared to an average area of $0.85\ cm^2$ for males and $0.53\ cm^2$ for females [40]. All the values from the reference are based on cadaver measurements. Exact dimensions on the entire sample used in this work can be found in Corcoran and Chigier [39].

A steady flow was maintained through the model using a downstream suction source. The spray from a medical nebulizer was added to the flow upstream of the model. The nebulizer served: (1) to simulate the conditions during an inhalation treatment, (2) to provide spray droplet seeding for velocimetry, and (3) to administer the liquid dye used for deposition testing. A previous cadaver based model which was identical to the one mentioned above except that it did not include a carinal cast, is also mentioned within the results. Complete results from this model have been previously reported [39].

Velocimetry was performed using an Aerometrics Phase Dop-

pler Particle Analyzer (PDPA). The measurement region of this instrument is formed by the intersection of 2 laser beams. As droplets pass through this intersection, they produce scattering signals that can be interpreted by a receiver focused on the intersection. Measurements of droplet size and velocity can be obtained for each droplet passing through the measurement region.

Velocimetry

Measurements were made at two different steady flow rates: 18.1 LPM and 41.1 LPM. Based on tracheal diameter, these flow rates correspond to Reynolds numbers of 1700 and 4000. (Reynolds number: $Re=\rho VD/\mu$, where ρ is air density, V is air velocity, D is a geometric parameter of the model and μ is air viscosity.) Flow rates were calculated by averaging the axial velocity measurements made at the most downstream location and multiplying by flow area. Reynolds number values were based on a velocity measurement made at the centerline of the trachea, 4 diameters downstream of the first accessible measurement region beneath the glottis. For the $Re_{trachea}=1700$ case the nebulizer was operated at 15 psig and 5.3 LPM. For the $Re_{trachea}=4000$ case, the nebulizer was operated at 28 psig and 8.4 LPM.

An array of thirty-three measurements was made at each of five downstream locations, beginning approximately 1 cm beneath the glottal plane and proceeding along the length of the trachea to just above the carina. (The specific measurement locations were 0, 2, 4, 5.5 and 6 tracheal diameters downstream of the glottis.) The measurement points were spread evenly throughout the circular area as depicted in Fig. 1. Traversing of the model was performed to make the measurement at each point. Model movement in 3 dimensions was performed using a precision traversing system. The system x-axis was aligned as best as possible to a posterior-anterior line along the center of the lumen of the vocal folds. Negative x coordinate values correspond to the anterior side of the model.

At each point the PDPA measured the axial velocity of approximately 20000 successive droplets. This velocity data was then used to compute the average velocity (V_{ave}) and the root-mean squared velocity (V_{rms}) at that point. Axial turbulence intensity was also calculated ($\sigma=V_{rms}/V_{ave}$). Average velocity and turbulence intensity data was represented in contour form, where the contour lines represent levels of constant axial velocity or turbulence intensity. The contours presented in the results section were produced using program SAS (SAS Institute Inc., SAS Campus Drive, Cary, North Carolina 27513). Zero data representing the outer boundary of the tube was added to incorporate the boundary conditions caused by the walls.

For all of these experiments the Phase Doppler Interferometer used was the phase Doppler Particle Analyzer (PDPA, Aerometrics/TSI, St. Paul, MN). The collection angle was set to 45 degrees. A transmitter with a beam expander and a 238.6 mm lens was used. The receiver was also equipped with a 238.6 mm lens. A data collection rate of 40 MHz was used. Laser power varied between 1 and 1.25 watts. A single pair of beams in a plane parallel to the axis of the tracheal tube was used to make velocity measurements. The second beam pair was not utilized since the curvature of the glass in that plane will result in a split probe volume. This prevents measurement of the two velocity components at the same point, at the same time. Some deflection of the axial beam pair will occur as well due to its passage through the glass. Through calculations based on Durst et al. [41], it was determined that the potential deflection of the laser beam intersection from its intended location would be of the order of 0.3 mm, which is negligible relative to the scale of measurement.

The numerical average diameter of these droplets was approximately 1.9 μm. Seed particles with diameters of 1.0-1.5 μm are often utilized for Laser Doppler Velocimetry experiments utilizing air as the medium [42–45]. It is proposed that a minor amount of lag was present due to the use of droplets slightly larger than ideal size, but that this lag was relatively inconsequential for this steady flow experiment.

Table 1 Physical characteristics of sprays used for fluorescent deposition testing as compared to water sprays from the same devices.

Nebulizer	Liquid	Mass Median Diameter	Valid % of Measurement	Valid Count
Hudson	Water	3.3	82.0	33192
Hudson	Dye	3.2	81.9	31592
Prototype	Water	1.8	83.8	16706
Prototype	Dye	1.9	84.1	16817

Deposition Testing

A qualitative representation of deposition within the model was obtained through the use of a fluorescent aerosol. A dye solution was produced by mixing 25 parts water to 1 part of Van Aken Jazz Fluorescent Yellow Tempera Poster Paint (Van Aken Int., Rancho Cucamonga, CA). The mixture takes the form of a fluorescent yellow suspension.

A spray generated using this fluorescent yellow dye was administered through the model. The experiment was run through the complete nebulization of four 6 ml doses of the fluorescent dye. Prior to the administration of the dye, the entire apparatus was externally sprayed with anti static spray. After the experiment two 75 W black lights were used to illuminate the tracheal section of the model. The black lights cause the yellow dye to exhibit enhanced fluorescence, making it more visible.

After the conclusion of the experiment, photographs were taken of the tracheal model. These photographs were developed and scanned. In order to enhance the appearance of the dye, the photographs were brightened using Adobe PhotoShop (Adobe Systems Inc., San Jose, CA). The brightening (level=50) was performed on the whole image, after which the background colors were replaced with absolute black to further emphasize the appearance of the dye.

The fluorescent sprays were produced using two different nebulizers. A Hudson MicroMist operating at 30 psig and 8 LPM was utilized for all flow rate comparisons. A prototype nebulizer operated at 50 psig and 8 LPM was used to generate a smaller MMAD spray as required to determine the effect of droplet size on deposition.

The Phase Doppler Interferometer was utilized to characterize both nebulizers, operated as described above administering both plain water and the dye solution. This was done to ensure that the dye sprays were characteristic of typical medicinal sprays. Table 1 lists the corresponding sizes and validation data obtained from the PDPA. These PDPA measurements were made outside of any glass enclosures and utilized both of the instruments beam pairs.

Results

Figure 2 presents the axial velocity and axial turbulence intensity contours noted at three positions downstream of the larynx for an air flow rate of 18.1 LPM/$Re_{trachea}=1700$. In this case the velocity contour interval is 0.5 m/s and the turbulence intensity contour is 0.2. A strong jet is notable in the right anterior trachea. The peak velocity noted in the right-anterior trachea was 4.23 m/s. A region of reverse flow is notable in the left trachea as represented by the dotted contour lines. The peak reverse flow velocity was 0.99 m/s. The jet sustains in the right side of the trachea through at least 6 downstream diameters. At 6 downstream diameters the maximum jet velocity noted was 2.09 m/s. The (x,y) position of this downstream maximum was within 2 mm of the position of the peak velocity noted at the furthest upstream position. The average axial velocity at 6 diameters downstream was 1.78 m/s. Peaks of high axial turbulence intensity are typically found at the interface

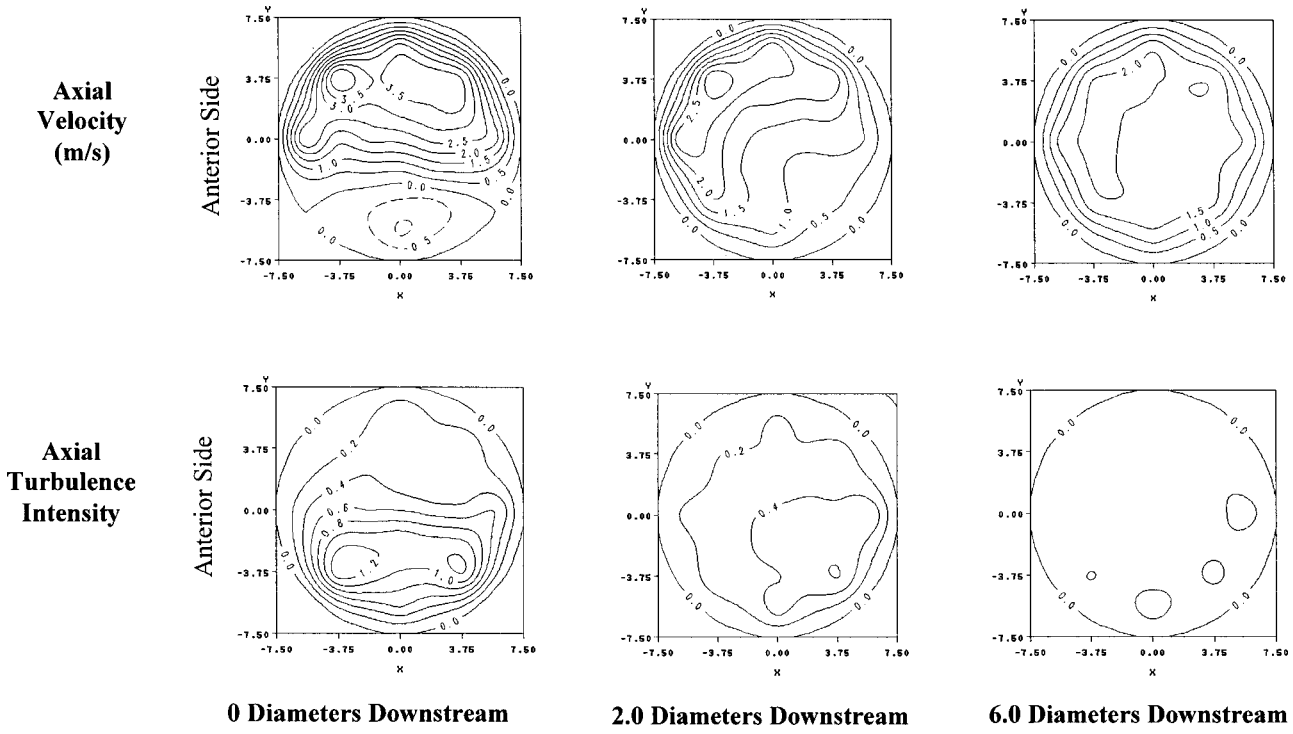

Fig. 2 Axial velocity and turbulence intensity contours for Q=18.1 LPM/$Re_{trachea}$=1700 case in the Larynx/Trachea/Carina model. Dotted contours represent reverse flows. The contour interval for velocity is 0.5 m/s. The contour for axial turbulence intensity is 0.2 (dimensionless).

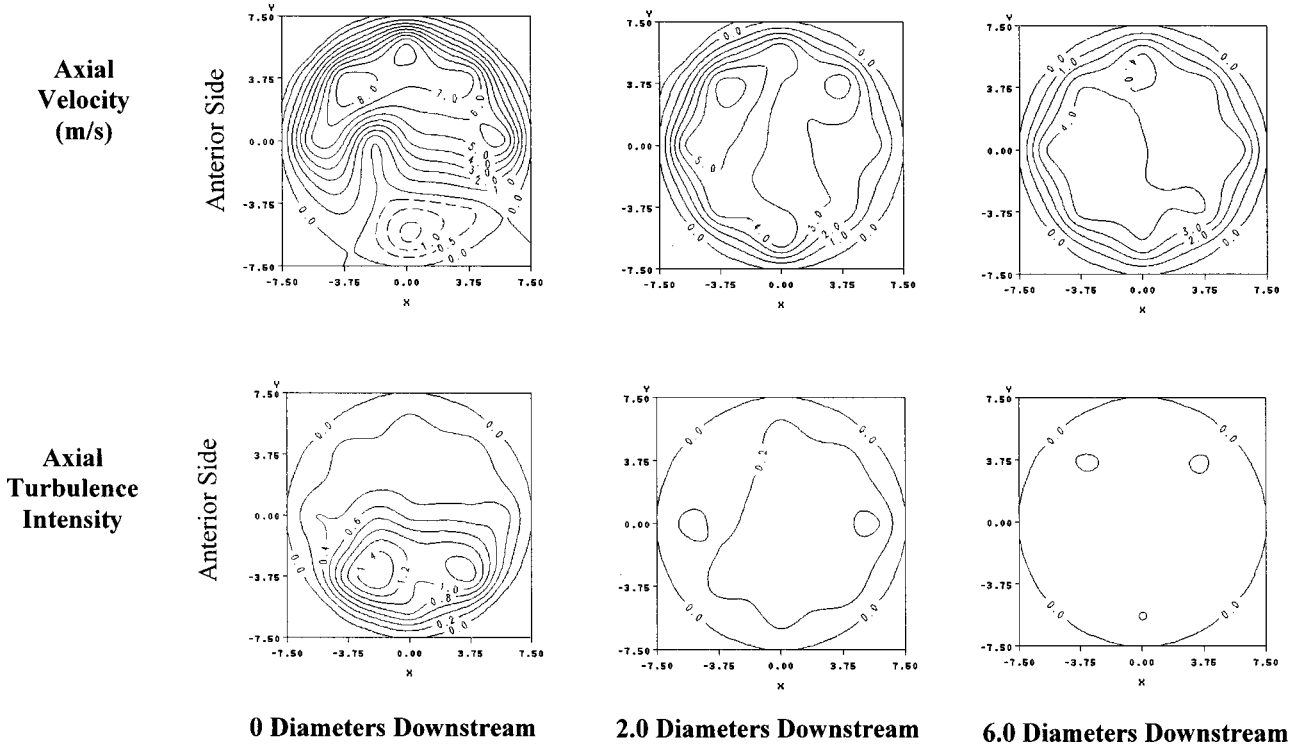

Fig. 3 Axial velocity and turbulence intensity contours for Q=41.1 LPM/$Re_{trachea}$=4000 case in the Larynx/Trachea/Carina model. Dotted contours represent reverse flows. The contour interval for velocity is 1.0 m/s for the positive axial flows and 0.5 m/s for the reverse flows. The contour interval for turbulence intensity is 0.2 (dimensionless).

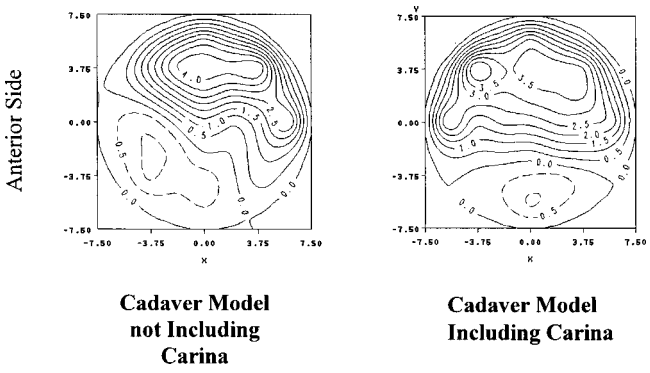

Fig. 4 Velocity contours immediately downstream of the glottal constriction from two different models examined at $Re_{trachea}=1700$. The first model is a cadaver-based cast model with a cast larynx and a round trachea. The next model uses the same cast larynx and round trachea, but includes also a casting of the carina. Note how this downstream element affects the upstream flows.

between the jet and the reverse flow regions. Two peaks are particularly notable in the left side of the trachea just downstream of the vocal folds. Axial turbulence intensity appears to quickly decay.

These results do bear strong resemblance to the contours reported by Olson which were based on hot wire anemometry [14]. Those tests were done at a somewhat higher flow rate (30 liters/min vs. 18 liters/min). The instrumentation used by Olson would not have been able to differentiate any reverse flows. The reverse flows reported in Fig. 2 are simply reported as low-flow regions in Olson's work. Reverse flow regions are noted downstream of the vocal folds as described in the computation models [28,29]. The orientation of the jet and the reverse flow regions appears to be quite different however, likely owing to their use of an oval representation of the vocal and vestibular folds, vs. the triangular shape of this region in the current model. The computational model of Renotte et al. [32] utilized a triangular orifice and produced a pattern more similar to the current model with reverse flows persisting as far as 2 diameters downstream.

Figure 3 presents axial velocity and turbulence intensity data for a higher flow case: $Q=41.1$ LPM/$Re_{trachea}=4000$. A high speed jet is apparent on the right side of the trachea. The maximum velocity noted in this region was 7.97 m/s. The maximum reverse flow velocity noted was 1.51 m/s. At the furthest downstream location the maximum axial velocity noted was 4.40 m/s. The average axial velocity at this level was 3.87 m/s. Regions of high turbulence intensity are again notable on the left side of the trachea near where the high-speed jet flow interfaced with the reverse flow region. The turbulence intensity in this case appears to dissipate even more quickly than in the previous lower speed case.

Again these contours bear resemblance to Olson's work [14]. Peak velocities noted in Olson's 36 liters/min case also closely resemble those measured here ($\sim$8 m/s, downstream of the glottis). The computational works [28–32] included a variable lumen in the larynx. Though the lack of a variable lumen in the current model limits its applicability, the comparability with Olson's work attests to its applicability in the two flow cases considered.

Figure 4 presents velocity contours measured immediately

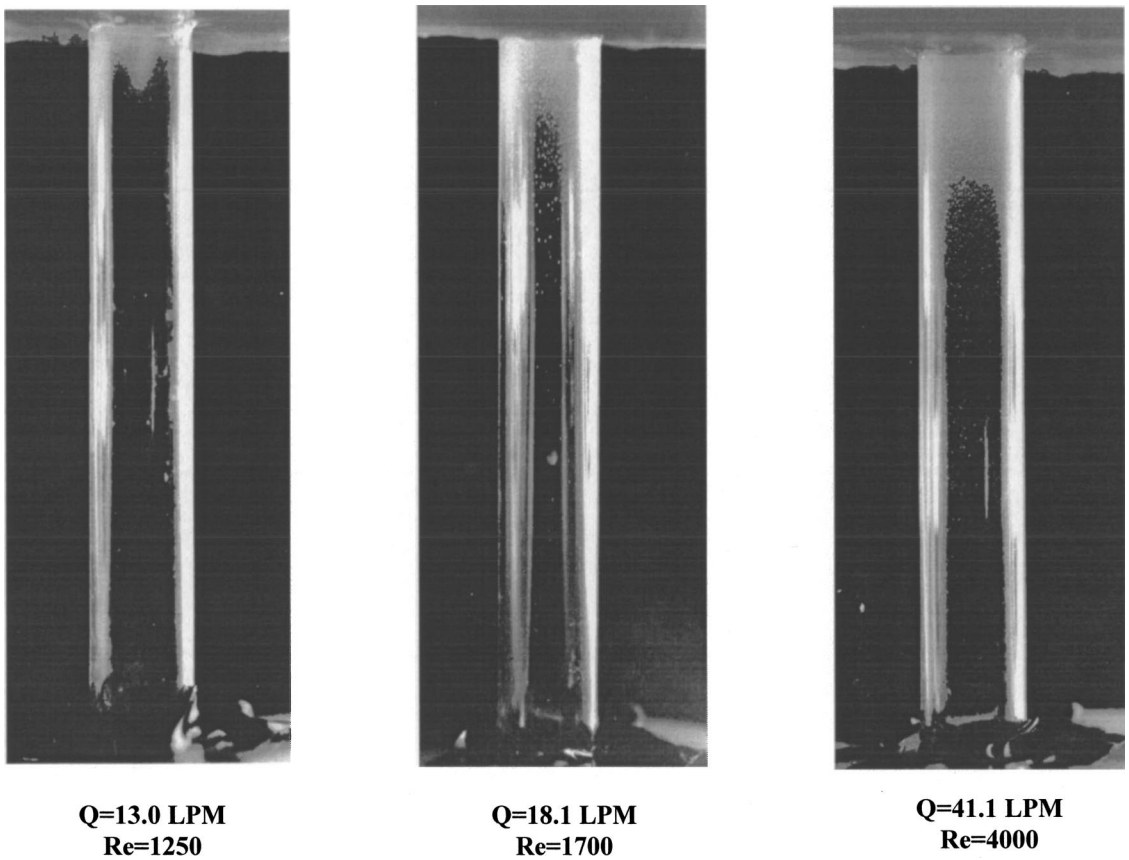

Fig. 5 Tracheal deposition depicted through the use of fluorescent dye. For each steady flow inhalation case a nebulizer was allowed to run to completion from 6 ml, 4 times. Images above depict the anterior side of the trachea which demonstrated high levels of deposition. Nebulizer operating conditions were identical for the three cases.

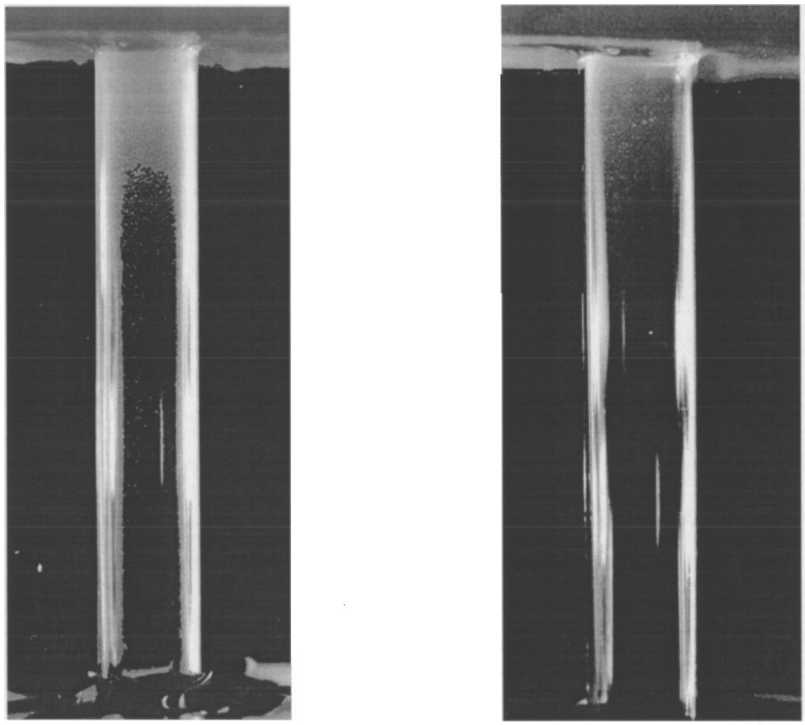

Fig. 6 Spray deposition variation for different sized sprays. The same total volume of dye was administered through the model in both cases.

downstream of the glottises of two different throat models at Q = 18.1 LPM. The models were based on the same cadaver. One includes a cast larynx and a round trachea. The other includes a cast larynx, a round trachea and a cast carina. The carina appears to affect the upstream flow conditions. Specifically the carina mold causes the laryngeal jet to reposition into the right side of the trachea. This is due to the presence of a higher flow area on the right side of the carina. This example illustrates how downstream flow conditions in the airways can affect upstream flow conditions in the trachea.

Figure 5 presents tracheal deposition images taken after fluorescent dye testing. This figure includes a low flow case along with the two flow cases previously discussed. What is depicted is

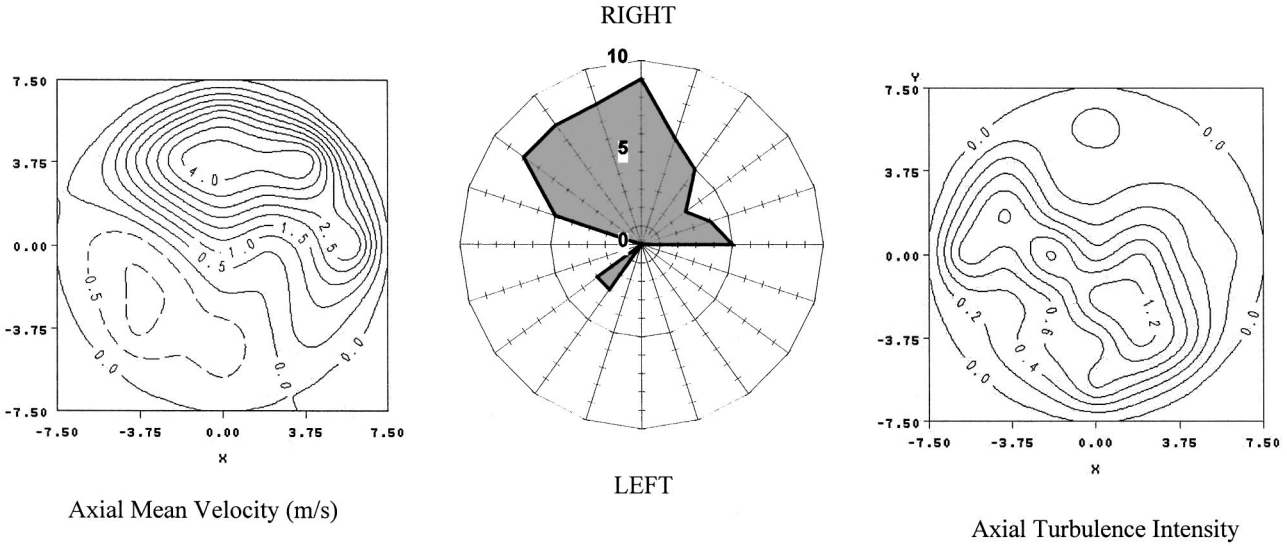

Fig. 7 Deposition levels around the circumference of the upper trachea compared to velocity and turbulence intensity contours at the same location. Deposition levels are plotted radially in the middle frame. A deposition level of 10 is considered highest and 0 lowest.

the glass tracheal portion of the model described in Fig. 1, after 4 doses of nebulized dye aerosol had been administered through the model. Note that significant deposition is present in the upper trachea, within approximately two diameters of the vocal folds. This agrees with the results of Schlesinger and Lippman [16], where the highest levels of deposition were reported within the first 3-4 cm of the trachea. The length of the trachea over which deposition is present increases with flow rate. Observation of the experiment also demonstrated an overall increase in total deposition with flow rate. It was also noted through observation that the highest levels of deposition were found in the right anterior portion of the upper trachea for all flow cases.

Figure 6 depicts the results of further dye testing conducted using two different size aerosols (Mass Median Diameters $=3.2$ and 1.9 μm, respectively). The same total amount of dye was administered through the model in each case. Deposition levels were significantly higher with the larger aerosol.

Figure 7 presents a comparison between deposition levels and axial velocity and turbulence intensity data measured in the upper trachea. The model used in this case included only a cadaver based cast larynx and a round trachea. The deposition levels were based on the judgement of an observer and plotted radially on a scale of 1 to 10 where 10 represents the heaviest deposition. Note that the highest levels of deposition correspond to regions where the laryngeal jet is found near the tracheal wall. There appears to be no obvious correspondence between deposition levels and turbulence intensity.

High right-anterior levels of deposition were noted in the models depicted in Figs. 4 and 5. Velocimetry data generated from these models demonstrates that the laryngeal jet passes near the tracheal wall at this location. (See Figs. 2 and 3.) The model depicted in Figs. 4 and 5 demonstrated little deposition on the left side of the trachea where turbulence intensity was the highest. Based on these results it appears that either there is no correspondence between turbulence intensity level and deposition level, or an inverse relationship between the two.

Discussion

A distinct axial velocity pattern is notable in both the simple and cadaver based throat models. This pattern includes the presence of a strong jet and a reverse flow region within approximately two tracheal diameters of the vocal folds. Peak axial velocities near the vocal folds were typically about twice the average velocities seen further downstream in the trachea. The locations of the jet and reverse flow regions within a given downstream plane in the trachea appeared to be dependent on the downstream conditions of the model. The addition of a cast carina to the model caused a shift in both the location of the jet and the location of the reverse flow region. In vivo, this implies that lung condition may have significant influence over flow conditions in the throat. Potentially this influence may even extend beyond the region examined. Dye testing performed in this study demonstrated that regions of high deposition within the trachea (i.e. tracheal hot spots) were typically found in locations where the laryngeal jet passed near the tracheal wall.

A simple mechanism could explain this phenomena. Spray droplets exiting the vocal folds will have radial and axial velocity components based on the expansion of the laryngeal jet and the bulk flow of the fluid. The combination of these components will result in trajectories that direct droplets towards the tracheal walls. The more inertial droplets will follow this trajectory and deposit through impaction while the less inertial droplets will be steered by drag forces back into the bulk flow preventing deposition. The physical behavior associated with the expansion implies a relationship between Stokes number and deposition level. Qualitative increases in deposition are noted with increased flow rate and droplet diameter both of which are components of the Stokes number. Past empirical correlations have demonstrated a relationship between tracheal deposition and Stokes number. This deposition increased in regions where the laryngeal jet was proximal to the tracheal wall because the droplets have a decreased radial distance to expand through prior to impaction. Since deposition is related to the location of the laryngeal jet within the trachea and the position of the laryngeal jet is related to the downstream conditions, it can be postulated that the downstream effects (i.e. lung conditions) could influence aerosol deposition in the trachea and possibly other locations upstream.

Very little deposition was noted on the tracheal walls in regions near peaks of high turbulence intensity. This implies either that turbulence has little effect on total deposition within the trachea, or that turbulence actually decreases deposition. The droplets transported by the turbulence are likely to be smaller. Correspondingly they will contain less dye mass and may be less notable during deposition testing. Inertial deposition mechanisms are likely to be more important than turbulence based mechanisms since the droplets subject to inertial deposition tend to be larger and carry more drug mass.

High peaks of axial turbulence intensity were noted immediately beneath the vocal folds typically at points where the jet interfaced with the reverse flow regions. These peak turbulence levels quickly decay along the length of the trachea. Only a few very small regions with turbulence intensities of the order of 0.2 were notable after 6 downstream diameters.

Acknowledgments

This work was funded by Sunrise Medical Home Healthcare Group of Somerset, PA.

References

[1] Boivin, G., Goyette, N., Hardy, I., Aoki, F., Wagner, A., and Trottier, S., 2000, "Rapid Antiviral Effect of Inhaled Zanamivir in the treatment of Naturally Occurring Influenza in Otherwise Healthy Adults," J. Infect. Dis., **181**(4), pp. 1471–1474.

[2] Iacono, A. T., Smaldone, G. C., Keenan, R. J., Diot, P., Dauber, J. H., Zeevi, A., Burckart, G. J., and Griffith, B. P., 1997, "Dose-Related Reversal of Acute Lung Rejection by Aerosolized Cyclosporine," Am. J. Respir. Crit. Care Med., **155**(5), pp. 1690–1698.

[3] Smaldone, G. C., and Palmer, L. B., 2000, "Aerosolized Antibiotics: Current and Future," Respiratory Care, **45**(6), pp. 667–675.

[4] Desai, M. H., Mlcak, R., Richardson, J., Nichols, R., and Herndon, D. N., 1998, "Reduction in Mortality in Pediatric Patients with Inhalation Injury with Aerosolized Heparin/N-Acetylcystine Therapy," J. Burn Care Rehabil., **19**(3), pp. 210–212. Also errata in **20**, 49.

[5] Laube, B. L., Benedict, G. W., and Dobs, A. S., 1998, "Time to Peak Insulin Level, Relative Bioavailability, and Effect of Site of Deposition of Nebulized Insulin in Patients with Noninsulin-Dependent Diabetes Mellitus," J Aerosol Med, **11**(3), pp. 153–173.

[6] Patton, J. S., Bukar, J., and Nagarajan, S., 1999, "Inhaled Insulin," Adv. Drug Deliv. Rev., **35**(2–3), pp. 235–247.

[7] Mather, L. E., Woodhouse, A., Ward, M. E., Farr, S. J., Rubsamen, R. A., and Eltherington, L. G., 1998, "Pulmonary Administration of Aerosolised Fentanyl: Pharmacokinetic Analysis of Systemic Delivery," Br. J. Clin. Pharmacol., **46**(1), pp. 37–43.

[8] Svartengren, K., Lindestad, P-Å, Svartengren, M., Philipson, K., Bylin, G., and Camner, P., 1994, "Deposition of Inhaled Particles in the Mouth and Throat of Asthmatic Subjects," Eur. Respir. J., **7**(8), pp. 1467–1473.

[9] Chua, H. L., Collis, G. G., Newbury, A. M., Chan, K., Bower, G. D., Sly, P. D., and Le Souef, P. N., 1994, "The Influence of Age on Aerosol Deposition in Children With Cystic Fibrosis," Eur. Respir. J., **7**(12), pp. 2185–2191.

[10] Diot, P., Palmer, L. B., Smaldone, A., DeCelie-Germana, J., Grimson, R., and Smaldone, G. C., 1997, "RhDnase I Aerosol Deposition and Related Factors in Cystic Fibrosis," Am. J. Respir. Crit. Care Med., **156**(5), pp. 1662–1668.

[11] Heyder, J., Gebhart, J., Rudolf, G., Schiller, C. F., and Stahlhofen, W., 1986, "Deposition of Particles in the Human Respiratory Tract in the Size Range 0.005-15 μm Range," J. Aerosol Sci., **17**(5), pp. 811–825.

[12] West, J. B., and Hugh-Jones, P., 1959, "Patterns of Gas Flow in the Upper Bronchial Tree," J. Appl. Physiol., **14**(5), pp. 753–759.

[13] Dekker, E., 1961, "Transition Between Laminar and Turbulent Flow in the Human Trachea," J. Appl. Physiol., **16**, pp. 1060–1064.

[14] Olson, D. E., Sudlow, M. F., Horsfield, K., and Filley, G. F., 1973, "Convective Patterns of Flow During Inspiration," Arch. Intern Med., **131**, pp. 51–57.

[15] Schlesinger, R. B., and Lippmann, M., 131, pp. 51–57, 1972, "Particle Deposition in Casts of the Human Upper Tracheobronchial Tree," Am. Ind. Hyg. Assoc. J., **33**(4), pp. 237–251.

[16] Schlesinger, R. B., and Lippmann, M., 1976, "Particle Deposition in the Trachea: In Vivo and in Hollow Casts," Thorax, **31**(6), pp. 678–684.

[17] Schlesinger, R. B., Bohning, D. E., Chan, T. L., and Lippman, M., 1977,

''Particle Deposition in a Hollow Cast of the Human Tracheobronchial Tree,'' J. Aerosol Sci., **8**, pp. 429–445.
[18] Martonen, T. B., 1983, ''Measurement of Particle Dose Distribution in a Model of a Human Larynx and Tracheobronchial Tree,'' J. Aerosol Sci., **14**, pp. 11–22.
[19] Martonen, T. B., 1983, ''Deposition of Inhaled Particulate Matter in the Upper Respiratory Tract, Larynx and Bronchial Airways: A Mathematical Description,'' J. Toxicol. Environ. Health, **12**(4–6), pp. 787–800.
[20] Chan, T. L., Lippman, M., Cohen, V., and Schlesinger, R. B., 1978, ''Effect of Electrostatic Charges on Particle Deposition in a Hollow Cast of the Human Larynx-Tracheobronchial Tree,'' J. Aerosol Sci., **9**, pp. 463–468.
[21] Martonen, T. B. and Lowe, J., 1983, *Aerosols in the Mining and Industrial Work Environments*, Ed. V.A. Marple and B. Liu, Ann Arbor Science, Chapter 13.
[22] Kim, C. S., and Fisher, D., 1999, ''Deposition Characteristics of Aerosol Particles in Sequentially Bifurcating Airway Models,'' Aerosol. Sci. Technol., **31**, pp. 198–220.
[23] Myojo, T., and Takaya, M., 2001, ''Estimation of Fibrous Aerosol Deposition in Upper Bronchi Based on Experimental Data with Model Bifurcation,'' Ind. Health, **39**(2), pp. 141–149.
[24] Cheng, Y-S., Zhou, Y., and Chen, B. T., 1999, ''Particle Deposition in a Cast of Human Oral Airways,'' Aerosol. Sci. Technol., **31**, pp. 286–300.
[25] Wroblewsi, D. E., and Choi, Y., 1998, ''Characteristics of Glottis-Induced Turbulence in Oscillatory Flow,'' J. Biomech. Eng., **120**(2), pp. 217–226.
[26] Martonen, T. B., 1993, ''Mathematical Model for the Selective Deposition of Inhaled Pharmaceuticals,'' J. Pharm. Sci., **82**(12), pp. 1191–1199.
[27] Martonen, T. B., Zhang, Z., and Lessmann, R. C., 1993, ''Fluid Dynamics in the Human Larynx and Upper Tracheobronchial Airways,'' Aerosol. Sci. Technol., **19**, pp. 133–156.
[28] Katz, I. M., and Martonen, T. B., 1996, ''Flow Patterns in Three Dimensional Laryngeal Models,'' J. Aerosol Med., **9**(4), pp. 501–511.
[29] Katz, I. M., and Martonen, T. B, 1996, ''Three Dimensional Fluid Particle Trajectories in the Human Larynx and Trachea,'' J Aerosol Med, **9**(4), pp. 513–519.
[30] Katz, I. M., and Martonen, T. B, 1997, ''Three Dimensional Computational Study of Inspratory Aerosol Flow Through the Larynx: The Effect of Glottal Aperture Modulation,'' J. Aerosol Sci., **28**, pp. 1073–1083.
[31] Katz, I. M., Davis, B. M., and Martonen, T. B., 1999, ''A Numerical Study of Particle Motion within the Human Larynx and Trachea,'' J. Aerosol Sci., **30**, pp. 173–183.
[32] Renotte, C., Bouffioux, V., and Wilquem, F., 2000, ''Numerical 3D Analysis of Oscillatory Flow in the Time-Varying Laryngeal Channel,'' J. Biomech., **33**(12), pp. 1637–1644.
[33] Gemci, T., Corcoran, T. E., and Chigier, N., 2002, ''A Numerical and Experimental Study of Spray Dynamics in a Simple Throat Model,'' Journal of Aerosol Science and Technology, **36**(1), pp. 18–38.
[34] Gemci, T., Corcoran, T. E., Yakut, K., Shortall, B. and Chigier, N., 2001, ''Numerical Simulation of Particle and Air Velocity Fields in a Model of a Cadaver Throat,'' *Proc. Institute for Liquid Atomization and Spray Systems-North and South America, Dearborn, MI*.
[35] Gemci, T., Corcoran, T. E., Yakut, K., Shortall, B. and Chigier, N., 2001, ''Spray Dynamics and Deposition of Inhaled Medications in the Throat,'' *Proc. Institute for Liquid Atomization and Spray Systems-Europe, Zurich, Switzerland.*
[36] Martonen, T. B., Yang, Y., and Xue, Z. Q., 1994, ''Effects of Carinal Ridge Shapes on Lung Airstreams,'' Aerosol. Sci. Technol., **21**, pp. 119–136.
[37] Martonen, T. B., Yang, Y., and Xue, Z. Q., 1994, ''Influences of Cartilaginous Rings on Tracheobronchial Fluid Dynamics,'' Inhalation Toxicol., **6**, pp. 185–203.
[38] Martonen, T. B, Musante, C. J., Segal, R. A., Schroeter, J. D., Hwang, D., Dolovich, M. A., Burton, R., Spencer, R. M., and Fleming, J. S., 2000, ''Lung Models: Strengths and Limitations,'' Respiratory Care, **45**(6), pp. 712–736.
[39] Corcoran, T. E., and Chigier, N., 2000, ''Characterization of the Laryngeal Jet Using Phase Doppler Interferometry,'' Journal of Aerosol Medicine, **13**(2), pp. 125–137.
[40] Eckel, H. E., and Sittel, C., 1995, ''Morphometry of the Larynx in Horizontal Sections,'' Am. J. Otolaryngol., **16**(1), pp. 40–48.
[41] Durst, F., Melling, A., and Whitelaw, J. H., 1981, *Principles and Practice of Laser-Doppler Anemometry*, 2nd Edition, Academic Press, London.
[42] Belmabrouk, H., and Michard, M., 1998, ''Taylor Length Scale Measurement by Laser Doppler Velocimetry,'' Exp. Fluids, **25**, pp. 69–76.
[43] Tagawa, M., Nagaya, S., and Ohta, Y., 2001, ''Simultaneous Measurement of Velocity and Temperature in High-Temperature Turbulent Flows: A Combination of LDV and Three-Wire Temperature Probe,'' Exp. Fluids, **30**, pp. 43–152.
[44] Wilson, S. H., and Lee, O. K. L., 1985, ''Laser Anemometry in a Research Engine with a Single Central Valve,'' *International Conference on Laser Anemometry-Advances and Application, 12/85, Manchester, UK*.
[45] Menon, R. and Lai, W. T., 1991, ''Key Considerations in the Selection of Seed Particles for LDV Measurements,'' *Fourth International Conference on Laser Anemometry, 8/91, Cleveland, OH*.